Experimental Investigation on Energy Dissipation Subsidiary Piers for Long Span Cable-Stayed Bridges

Limin Sun, Jun Wei & Wen Xie
StateKeyLaboratory for DisasterReductionin Civil Engineering, TongjiUniversity, China

SUMMARY:
The seismic performance of long span cable-stayed bridge is strongly dependent on structural systems. Based on the investigation on the seismic damage mechanisms of long span cable-stayed bridges in longitudinal direction, the new structural systems with damage control strategies of sacrificing subsidiary piers were proposed and the required capacity for the piers was calculated. Then, 1/10 scaled models for three types of subsidiary pier were tested bycyclical loadin horizontal. All the models were reinforced concrete columns with rectangular hollow sections. One of them was a single column pier, while the others weretwin-column piers equipped by shear links or buckling restrained braces for energy dissipation. The failure patterns, the effects of ductility and the energy dissipation of the piers were discussed. The influences of energy dissipation members on the performance of subsidiary piers were investigated. An analytical investigation was conducted to replicate the experimental results of the subsidiary piers.

Keywords: Experiment, long span cable-stayed bridge, subsidiary piers, energy dissipation

1. INTRODUCTION

In recent years, China is planning several sea-crossing projects consisting of long span bridges, which have low natural frequencies. Many of those bridges are located in areas of high seismicity, and are likely subjected to severe damage or even collapse under strong earthquakes. In order to decrease the losses caused by strong earthquakes, it is significant to propose a new structural system with reliable mechanisms to dissipate seismic energy both for structural safety as well as reducingforces in structural members. The conceptof anew structural system is, by designing sacrificial members to dissipate the seismic energy, the integrity of main components can be preserved, which is known as the concept of damage control. The concept of “damage-controlled structures or damage-tolerant structures”waspropose by Wada et al.(1994)before the Northridge earthquake in the USA in 1994. Since Hyogoken-Nanbu earthquake in Japan in 1995, damage-controlled structures have been dramatically implemented in practice in Japan (Huang et al. 2002). A damage-controlled structure is defined as a combination of several structural systems and energy dissipation devices that are integrated in such a way as to restrict damage to a specific set of structural elements that can be readily repaired. The primary structure can be protected from damage and can remain in continuous use even after an extreme earthquake. Connor et al. (1997) demonstrated that the effectiveness of this structural concept depends on the energy dissipation capacity of the braces and on the ability of the primary structure to remain elastic during the motion associated with a major seismic event. McDaniel et al. (2005) studied the influence of inelastic tower links on the seismic response of the cable-supported bridges. The addition of inelastic links to the tower improved the behaviour of the structure. Cho et al. (2008) proposed a Bi-Directional Energy-Dissipating Sacrificial Device as a solution for enhancement of seismic performance of a bridge, which can significantly decrease the shear forces of the piers and reduce the relative motions in bridges. EI-Bahey et al. (2012) investigated the hysteretic behaviour of bridge piers with structural fuses and Bi-steel columns and compared the effect of different types of structural fuses on accelerated bridge construction bridge bents. The energy dissipation members adopted in this studyare shear links (SLs) and buckling restrained braces (BRBs).

2. PROTOTYPE BRIDGE AND SPECIMEN

The prototype bridge considered is a trial designed cable-stayed bridge having a main span of 1400mand seven spans with a total length of2672m(150m+176m+310m+1400m+310m+176m+150m), as shown in Fig. 2.1. There are two subsidiary piers and oneside pier at each side span. The height of the tower is 357m and the pier is 60m. The two A-shaped towers are made of reinforced concrete. The subsidiary piers are designed originally as reinforced concrete hollow rectangular columns. A total of 304 stay cables splay out in semi-harp configuration. The floating superstructure is comprised of steel box girder with a width of 41m.

Limin Sun et al (2010) proposed a new structural system with a damage control strategy which was based on the simulation results of the cable-stayed bridge mentioned above. The damage control strategy under an extremely strong earthquake, the peak ground acceleration of which is 1.0g, is to reduce the damage of the towers by sacrificing the subsidiary piers. The recommended elastic stiffness and base shear yielding strength of the subsidiary piers are 60MN/m and 18MN, respectively. The capacity of the subsidiary piers can satisfy the demand of damage control.

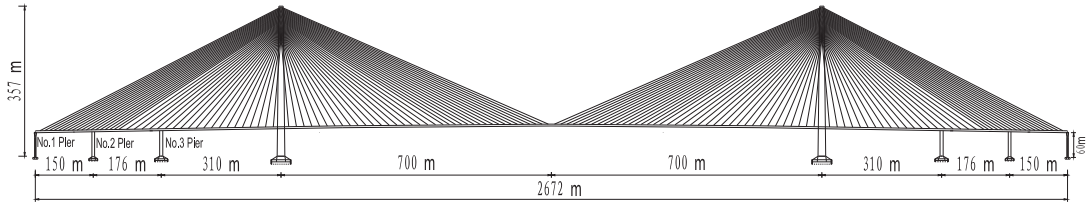

Figure 2.1. Elevation of 1400m cable-stayed bridge

To assess the damage control strategy, three types of 6m high subsidiary pier specimens in 1/10 scale were designed. The cross section and elevations of all three specimens with reinforced concrete rectangular hollow sections are shown in Fig.2.2.The wall thickness of the specimens is 150mm. The first specimen is a single column pier (labelled as SRC), the cross section of which is 850mm×1050mm, while the other twoare twin-column piers with two 850mm×520mm cross sections. On the second specimen, SLs are installed between the twocolumns to serve as a series of energy dissipation members (labelledas TRC-SL). Thethird specimen uses BRBs as the series of energy dissipation members between the two columns (labelledas TRC-BRB).The photographs of specimens TRC-SL and TRC-BRB are shown in Fig. 2.4.

Table 2.1. Compressive Test Results Of Concrete

Specimen	Cube compressive strength(MPa)	Modulus of elasticity($\times 10^4$MPa)
SRC	32.4	3.06
TRC-SL	35.4	3.14
TRC-BRB	33.0	3.08

On the top of the specimens TRC-SL and TRC-BRB, the two reinforced concrete columnsare connected by a hinge bar horizontally to eliminate moment and shear at the connection points and to obtain maximum deformation of the energy dissipation members when the specimen deforms. While the welded connections areused to attach the energy dissipation members to the embedded parts in the reinforced concrete columns. The spacing of the energy dissipation members is 1m. Two parallel SLs were horizontally connected to the columnsatthe same height, while two parallel BRBs were connected to the columns by the angle of 45 degree atthe same height. The embedded parts and its full penetration welds are designed to remain elastic during the experimental procedure.

The geometry and photograph of the SL are shown in Fig. 2.3(a). The SL is built-up steel wide-flange sections with a shear deformable region at the middle and the connection region ofboth ends, designed

to yield in shear. The cross-section dimensions are varying along the longitudinal direction of the SL. The SL flange is 130mm wide. The flange thickness varies from 10mm in the deformable region to 15mm in the connection region. The web thickness varies from 5mm in the deformable region to 10mm in the connection region, with a clear height of 100mm.

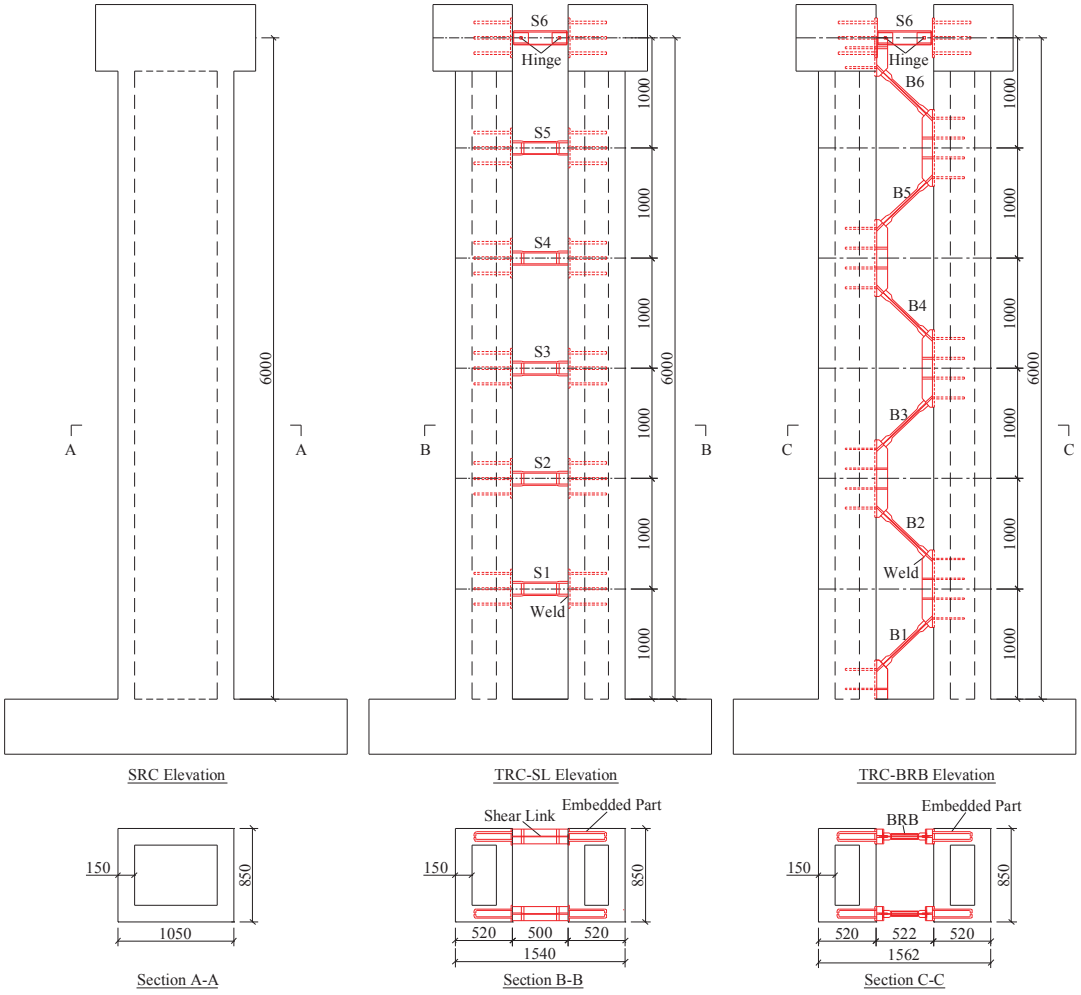

Figure 2.2. Specimen cross section and elevations (unit: mm)

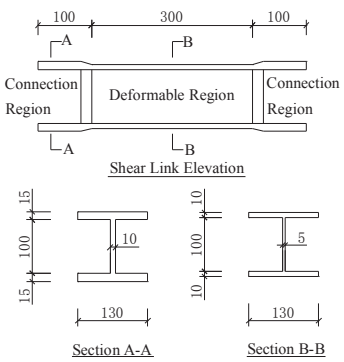

(a)

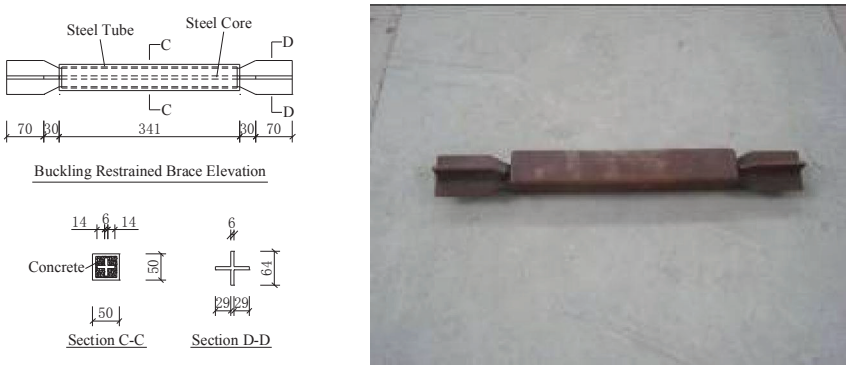

(b)

Figure 2.3. Geometries and photographs of energy dissipation members: (a) SL; (b) BRB (unit: mm)

The geometry and photograph of the BRB are shown in Fig. 2.3(b). The BRBs consist of a cross-shaped steel core encased in a steel tube filled with concrete, designed to yield in axial force. The steel core carries the axial load while the outer tube, via the concrete, provides lateral restraint to the core and prevents local buckling of the yielding core when in compression. A thin layer of an unbounded material along the steel core/concrete interface eliminates shear transfer during the elongation and contraction of the steel core and also accommodates its lateral expansion when in compression. The steel core thickness is 6mm, and the wall thickness of the rectangular hollow steel tube is 5mm. The steel core width varies from 64mm outside the tube on both ends to 34mm into the tube at the middle.

For each specimen, the concrete cube compressive strength and the modulus of elasticity from compressive coupon tests are presented in Table 2.1. Monotonic tensile coupon test results for the steel used in fabrication of the columns, SLs and BRBs are presented in Table 2.2. SLs and BRBs are made of low yielding point steel plates.

Table 2.2. Tensile Test Results Of Steel

Steel	Diameter or thickness (mm)	Yield strength (MPa)	Tensile strength (MPa)	Elongation (%)
Longitudinalrebar	12	364	538	31
Transverse rebar	10	338	462	30
flange of SL	10	285	444	-
Web of SL	5	275	386	-
Steel core of BRB	6	304	420	-

3. EXPERIMENTAL SET-UP AND LOADING METHOD

Three specimens under a constant axial force of about 25kN, were tested by a cyclical horizontal load. In the test set-up, the specimens were cast vertically with the reinforced concrete foundation and the reinforced concrete mass block that was fabricated on the top of columns to provide a constant axial load. A MTS servo-controlled static rated actuator that was horizontally mounted to a reaction wall was used to apply lateral load to the specimens. The actuator has a capacity of 1500kN and is capable to deformthe column 250mm in both push and pull directions, corresponding to a column drift (ratio of horizontal displacement to column height) of 4.2%.

The tests were conducted in a displacement controlled mode. A prescribed quasi-static cyclic loading sequence (see Fig. 3.1.) was imposed laterally to the top of the specimen until the tensile failure of longitudinal rebar at the bottom of the columns. In each case the displacement cycle was repeated three times to measure the strength degradation.

(a)

(b)

Figure 2.4. Photographs of specimens: (a) TRC-SL; (b) TRC-BRB

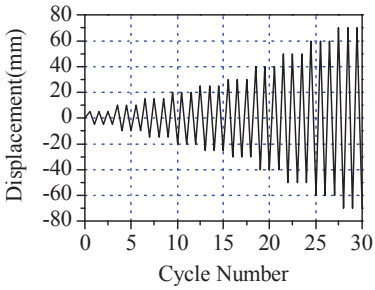

Figure 3.1. Loading protocol

The global displacements of the specimen were obtained from displacement transducer installed at different levels from the base to the top of the column. The strain of the rebar and concrete was obtained from stain gages installed at critical points (the surface of rebar and concrete at the bottom of each column), to determine whether these columns remain elastic during the tests. The average shear deformations of the SLs were computed from measurement of displacement transducers placed diagonally in the deformable region, and axial deformations of the BRBs were measured with displacement transducers installed in parallel with the braces and connected to the embedded parts. To verify if slippage or uplift occurred at the specimen base, horizontal and vertical transducers were installed on the foundation.

4. EXPERIMENTAL RESULTS

4.1 General Observations

All specimens developed stable responses up to certain displacement ductility levels. Horizontal cracks perpendicular to the column axis developed first in regions close to the bottom of the column. With the displacement increasing, the horizontal cracks became inclined and extended into the web zone of the column due to the influence of shear. At a stage exceeding the first yielding of the longitudinal rebar, independent shear cracks started to occur in the web zone. The failure modes of specimens SRC and TRC-SL were flexural failures, with plastic hinges formed at the bottom of the columns, while specimen TRC-BRB didn't reach the ultimate state due to limitation of working stroke of the MTS actuator.

The cracks of specimen SRC, which started to occur at a displacement of 10mm (0.17% drift), developed in the range of about 2m high from the base. At 28.6mm displacement (0.48% drift), signs of yielding were observed by strain gages installed on the longitudinal rebar at the bottom of the column. Up to 100mm displacement (1.67% drift), first signs of minor concrete spalling at the southwest corner of the bottom column were observed in the column base. The test continued for the specific purpose of observing the ultimate behaviour of the column. The rupture of the longitudinal rebar at the east side of the column started to occur at 190mm displacement (3.17% drift) as shown in Fig. 4.1, while concrete was crushed at the same drift level at the west side of the column as shown in Fig. 4.2. The load drop from maximum of 273.7kN to 218.5kN at that point, and then the test ended.

The cracks of specimen TRC-SL, which first occurred at a displacement of 15mm (0.25% drift), developed in the range of about 3m high from the base. At 24.8mm displacement (0.41% drift), signs of yielding started to occur on S5 (5^{th} row from the base). The longitudinal rebar started to yield at 40mm displacement (0.67% drift). Yielding had propagated to all SLs when 80mm (1.33% drift) displacement was reached. At 170mm displacement (2.83% drift), first signs of minor concrete spalling started to appear at southwest corner of the bottom west column. The web fracture of S5 was observed at 210mm displacement (3.5% drift) as shown in Fig. 4.3. The test continued until the

rupture of the longitudinal rebar started to appear at 240mm displacement (4% drift) as shown in Fig. 4.4. Then the test was terminated at that point.

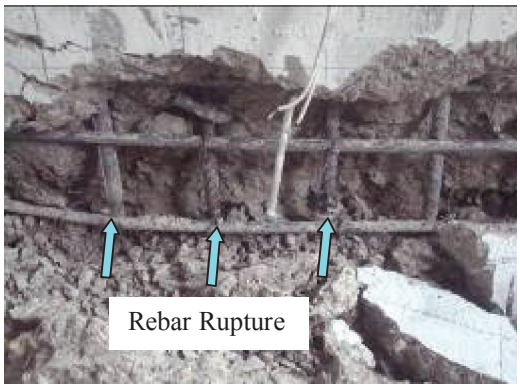

Figure 4.1. Longitudinal rebar rupture at the east side of specimen SRC at 190mm displacement

Figure 4.2. Concrete cover spalling at the west side of specimen SRC at 190mm displacement

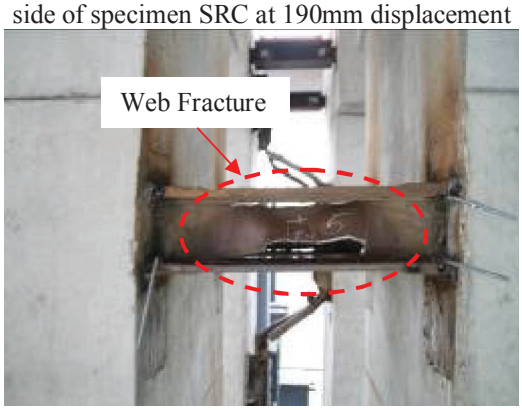

Figure 4.3. Web fracture of S5 at specimen TRC-SL at 210mm displacement

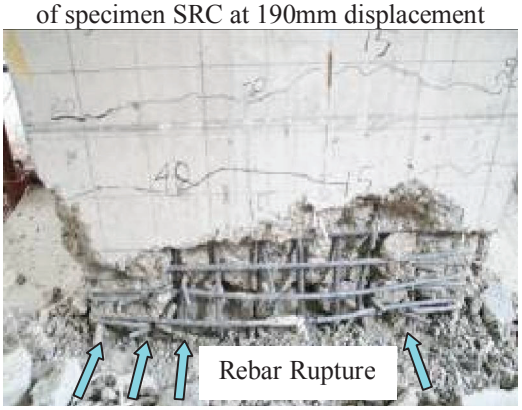

Figure 4.4. Longitudinal rebar rupture at the east side of specimen TRC-SL at 240mm displacement

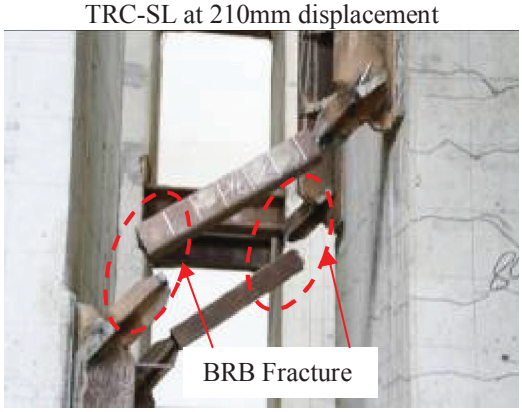

Figure 4.5. B2 fracture at specimen TRC-BRB at 240mm displacement

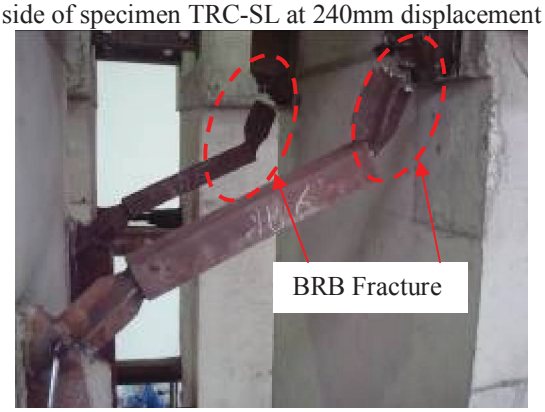

Figure 4.6. B6 fracture at specimen TRC-BRB at 110mm displacement

The cracks of specimen TRC-BRB were not observed until a displacement of 20mm (0.33% drift), which developed in the range of about 3m high from the base. Specimen TRC-BRB remained elastic up to a displacement equal to 14.4mm (0.24% drift). At that point, signs of yielding were observed by strain gages installed on the BRBs. Note that signs of yielding of the BRBs were earlier than concrete cracking. The yielding of the longitudinal rebar was observed at 40mm displacement (0.67% drift). Up to a displacement of 60mm (1.0% drift) yielding had propagated to all BRBs. The fracture of B6 (6^{th} row from the base) was observed at 110mm displacement (1.83% drift) as shown in Fig. 4.6. When 240mm displacement (4% drift) was reached, the fracture of B5 occurred as shown in Fig. 4.5. At that point only B4 and B2 remained working. The test continued up to 250mm displacement (4.2% drift)

which was limitation of working stroke of the MTS actuator. Signs of concrete cover spalling didn't appear at that point.

4.2 Ductility Factor and Dissipated Energy

The ductility factor is defined as the ultimate displacement Δ_m corresponding to the first rupture of the tensile longitudinal rebar in the descending portion of the horizontal load-displacement relationship divided by the yield displacement Δ_y at the occurrence of the first yielding of the longitudinal steel or energy dissipation members. Generally, the ultimate displacement Δ_m is defined as the displacement at 80 percent of the maximum lateral load P_m in the descending portion of the horizontal load-displacement relationship, but the method is not suitable to specimen TRC-BRB. Due to the failures of BRBs, the strength of specimen TRC-BRB reduces to 80 percent of the maximum lateral load P_m, but the columns don't reach the ultimate capacity. Hence specimen TRC-BRB is able to continue resisting the axial and horizontal load.

Table 4.1. Experimental results

Specimen	Δ_y (mm)			P_y (kN)			Δ_m (mm)			P_m (kN)			μ			E_D (MN.m)	Maximum Drift (%)
	+	-	Av.	+	-	Av.	+	-	Av.	+	-	Av.	+	-	Av.		
SRC	36.8	28.6	32.7	201.5	168.5	185.0	187.6	188.2	187.9	273.7	290.4	282.1	5.1	6.6	5.9	1.11	3.1
TRC-SL	22.1	27.4	24.8	193.9	210.0	202.0	240.0	239.6	239.8	414.5	418.3	416.4	10.9	8.7	9.8	4.98	4.0
TRC-BRB	14.4	14.6	14.5	137.4	171.9	154.7	249.7	249.8	249.8	354.1	358.3	356.2	17.3	17.1	17.2	2.33	4.2

Δ_y=yield displacement; P_y=yield lateral load; Δ_m=ultimate displacement; P_m=maximum lateral load; μ=displacement ductility factor; E_D=energy dissipation.

The dissipated energy is determined by integrating the areas bounded by all the hysteretic loops. Table 4.1.gives the experimental results of the ductility factor and dissipated energy for all specimens. It can be seen from Table 4.1.that the range of ductility factor for all specimens is from 5.9 to 17.2. When specimens TRC-SL and TRC-BRB are compared to specimen SRC, It can be seen that adding energy dissipation members can produce greater ductility factor and energy dissipation. The ductility factor of specimen TRC-BRB is larger than specimen TRC-SL, however, the energy dissipation of specimen TRC-BRB is less. It is because that the failures of BRBs appear earlier than the expected failures, which leads to much steeper degradation of the strength and stiffness.

Hysteretic loops and skeleton curves of the specimens SRC, TRC-SL and TRC-BRB are shown in Fig. 4.7. respectively. It can be seen that hysteretic loops of specimen TRC-SL are very plump compared to specimen SRC which behaves significant pinch effect. After the failures of BRBs, the energy dissipation capacity of specimen TRC-BRB is reduced with the degradation of the strength and stiffness. The cause of the failure is judged that the connection type of BRBs is not proper. Rigid connection type makes BRBs resist the unexpected moment which brings about much earlier fracture of BRBs.

4.3 Equivalent Viscous Damping Ratio

The damping of the specimens is provided by the inelastic deformation of reinforced concrete columns or energy dissipation members. Fig.4.8. presents the hysteretic energy-displacement relationship of all specimens. The hysteretic energy of the twin-column piers increases significantly than the single column pier due to the effect of additional energy dissipation members, however, the hysteretic energy of specimen TRC-BRB seriously reduces after the unexpected failures of BRBs. Hysteretic damping is conveniently expressed in the form of equivalent viscous damping for single degree of freedom oscillator. Equivalent viscous damping ratio can be seen as an index of the energy dissipation capacity

and is defined as the ratio of the dissipated energy in one cycle to the stain energy of an equivalent linearly elastic system as shown in Eqn. 4.1.(Priestley et al. 1995)

$$\xi_{eq,h} = \frac{A_h}{2\pi A_e} \tag{4.1}$$

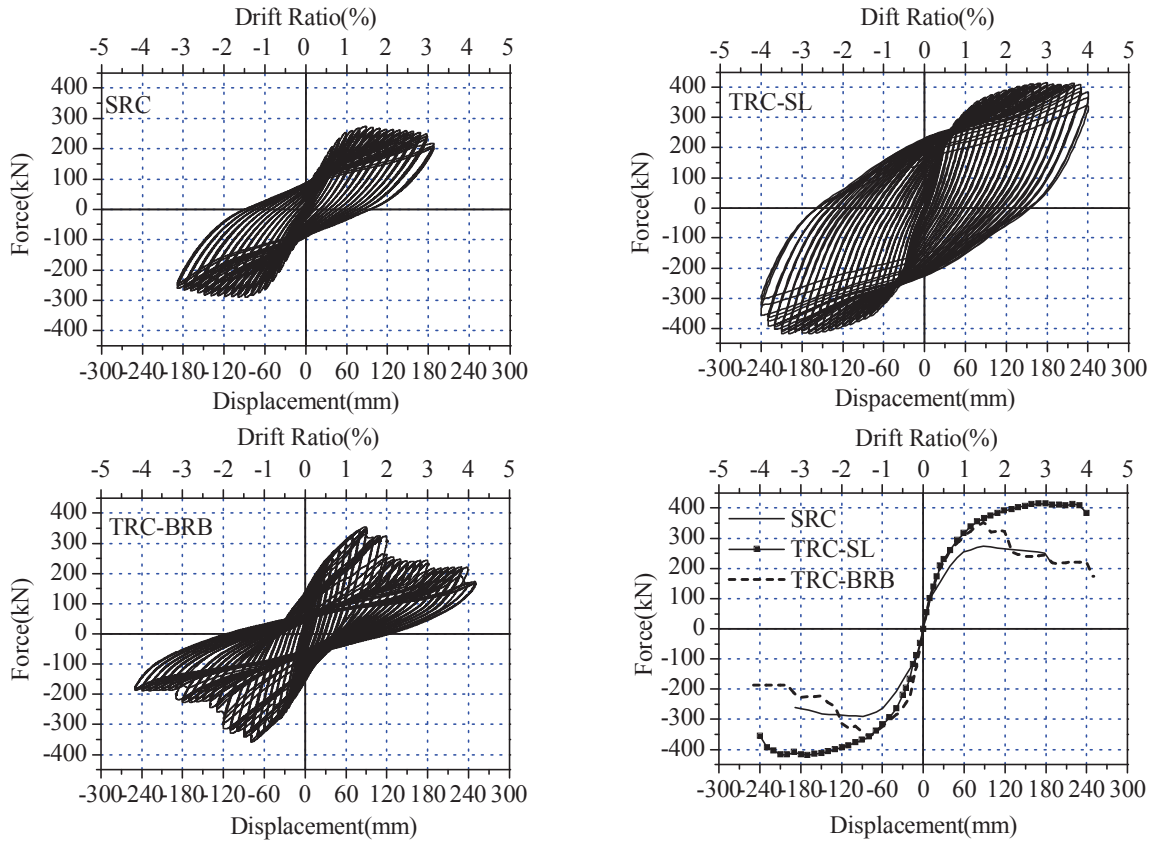

Figure 4.7. Hysteretic loops and skeleton curves of specimens

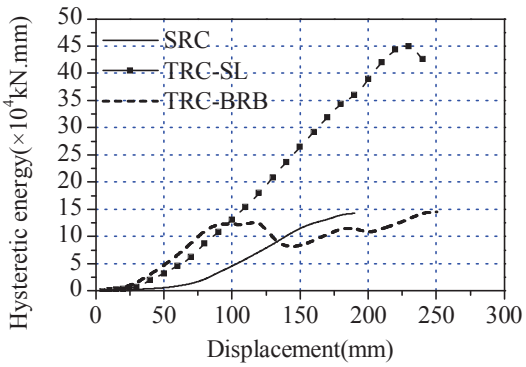

Figure 4.8. Hysteretic energy versus displacement relationship of specimens

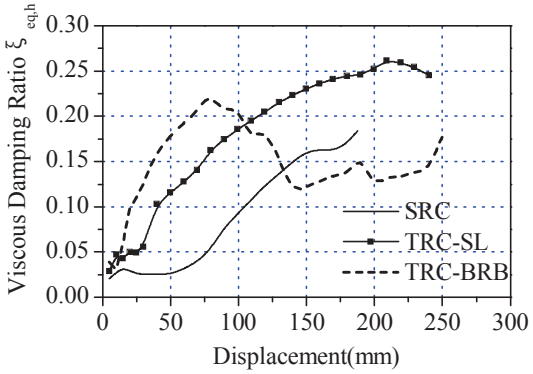

Figure 4.9. Viscous damping ratio versus displacement relationship of specimens

Where A_h = energy loss per cycle; A_e = elastic strain energy. Equivalent viscous damping ratio versus displacement relationship of all specimens is shown in Fig. 4.9. It can be seen that all specimens have similar capacities for the small levels of displacement. With displacement increasing, the values of specimens TRC-SL and TRC-BRB were much higher than the corresponding one of specimen SRC, but the damping ratio of specimen TRC-BRB started to decrease at 80mm displacement because of the unexpected failures of BRBs. Specimen SRC and TRC-SL exhibited

stable capacities of energy dissipation until failures, while the maximum value of specimen TRC-SL was 44 percent higher than the one of specimen SRC.

5. COMPARISION OF EXPERIMENTAL AND ANALYTICAL RESULTS

The numerical model was developed with the same geometrical and loading characteristics previously presented. The reinforced concrete columns, SLs and BRBs are modelled by fibre elements, with the interaction of moment and axial force considered. For the SLs, because shear behaviour dominates the response, inelastic shear behaviour should be taken into consideration in the fibre element. In what concerns the constitutive relations, for the concrete in compression the well known model of Mander et al. (1988) is adopted, with the effect of confinement due to the presence of stirrups considered. The model of Giuffré, Menegotto and Pinto is applied for the longitudinal rebar, along with the modifications introduced by Filippou et al. (1983). The model of bilinear elastic-plastic is used to simulate the behaviours of SLs and BRBs.

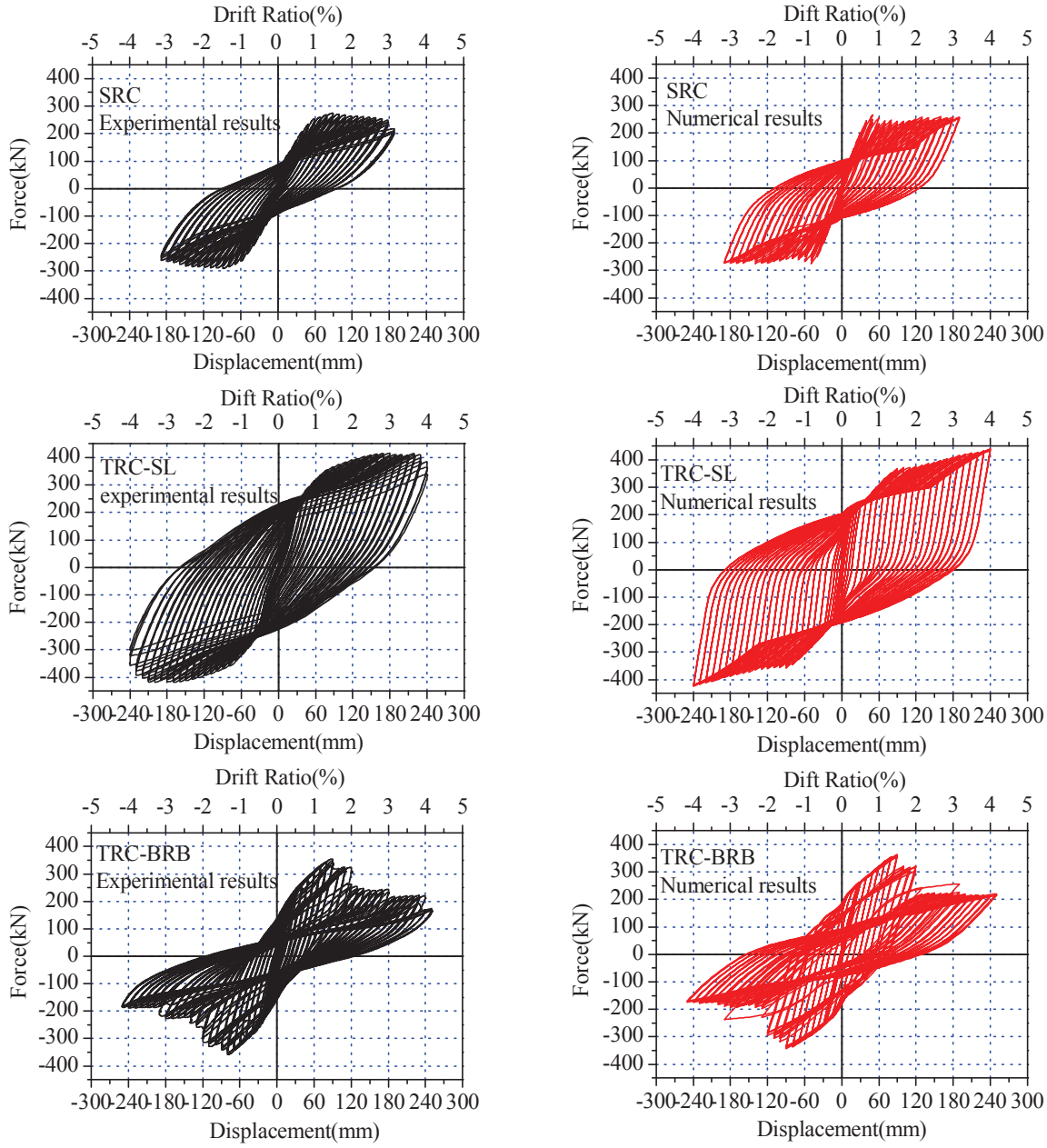

Figure.4.10. Hysteretic loops of specimens: comparison between the experimental and numerical results

The comparison of the load-displacement relationships from the experimental and numerical results of all specimens is shown in Fig.4.10. On the whole, the predictions from all specimens are similar to the test results, but some discrepancies are observed in the trend itself. It can be seen that the numerical results are in good agreement with the test data. After the yielding the discrepancies between the experimental and analytical results increase gradually, especially for the strength. The degradation of the strength is not well predicted in the plastic stage.

6. CONCLUSIONS

To validate whether the behaviors of energy dissipation of the subsidiary piers can satisfy the demand fordamage control of long span cable-stayed bridges, three 1/10 scaled specimens were tested. From the experimental results presented in this paper, the following conclusions can be drawn.

1) The effectiveness of energy dissipation for the specimens TRC-SL and TRC-BRB due to adding SLs or BRBs is very significant, compared to the specimen SRC. The hysteretic loops of the specimen TRC-SL are plump, while the hysteretic energy of specimen TRC-BRB decreases after the unexpected failures of BRBs.
2) The elastic stiffness and yielding strength of three prototype subsidiary piers can be obtained by inferring the experimental results. Except the yielding strength of specimen TRC-BRB, the other values can satisfy the demand of previously recommended design parameters.
3) Although some discrepancies exist, the analytical model can well predict the experimental results.
4) The potential capacity of energy dissipation for the specimen TRC-BRB is able to be improved if the BRBs and connection types are designed properly.

AKCNOWLEDGEMENT

The authors wish to thank the financial support provided by National Natural Science Foundation of China (Grant No.90915011).

REFERENCES

Wada, A. and Connor, J., et al. (1994). Damage Tolerant Structures. *Proceedings of: Fifth U.S-Japan Workshopon the Improvement of Structural Design and Construction Practices*, Applied Council Technology. 27-39.

Huang, Y. and Wada, A et al. (2002). Design of damage-controlled structures. Innovative Approaches to Earthquake Engineering. Billerica, MA: WIT Press.

Connor, J. and Wada, A et al. (1997). Damage-controlled structures. Ⅰ. Preliminary design methodology for seismically active regions. *JOURNAL OF STRUCTURAL ENGINEERING-ASCE.* **123:4**,423-431.

McDaniel, C. C. and Seible, F. (2005). Influence of Inelastic Tower Links on Cable-Supported Bridge Response. *JOURNAL OF BRIDGE ENGINEERING*. **10:3,**272-280.

Cho, K. and Kim, S. et al. (2008). A study on seismic performance of girder bridges equipped with bi-directional energy-dissipating sacrificial devices. *INTERNATIONAL JOURNAL OF STEEL STRUCTURES.* **8:1,**59-65.

El-Bahey, S. and Bruneau, M. (2012).Bridge Piers with Structural Fuses and Bi-Steel Columns.I: Experimental Testing. *JOURNAL OF BRIDGE ENGINEERING*. **17:1,**25-35.

Limin, S. and Wen, X. (2010). Damage Mechanism and Damage Control of Long Span Cable-Stayed Bridges Under Strong Earthquake. *Fifth World Conference on Structural Conrol and Monitoring*. **Session C-2:**108.

Priestley, M. J. N. et al. (1995). Seismic Design and Retrofit of Bridges, John Wiley &Sons, Inc.

Mander, J. B. and Priestley, M. J. N., et al. (1988).Theoretical stress-strain model for confined concrete. *JOURNAL OF STRUCTURAL ENGINEERING-ASCE.* **114:8,**1804-1826.

Filippou, F. C. and Popov, E. P. et al. (1983). Effects of Bond Deterioration on Hysteretic Behavior of Reinforced Concrete Joints. *EERC Report 83-19,* Earthquake Engineering Research Centre, Berkeley.